frontiers | Frontiers in Forests and Global Change

TYPE Original Research
PUBLISHED 17 July 2025
DOI 10.3389/ffgc.2025.1607871

OPEN ACCESS

EDITED BY
Azade Deljouei,
University of Florida, United States

REVIEWED BY
Abd Mujahid Hamdan,
UIN Ar-Raniry Banda Aceh, Indonesia
Katarzyna Dudzisz,
Polish Academy of Sciences, Poland
Bahia A. S. R. S,
São Paulo State University, Brazil

*CORRESPONDENCE
Haidong Wang
wanghd1210@163.com
Haixia Li
lhx4519@163.com

RECEIVED 08 April 2025
ACCEPTED 12 June 2025
PUBLISHED 17 July 2025

CITATION
Zhang X, Wang H, Liu H, Li H, Shi Y, Zheng G, Li F, Liu D, Jiang X, Ren E and Li G (2025) Vertical distribution and factors influencing tropical forest soil magnetic susceptibility in Xishuangbanna, Southwest China.
Front. For. Glob. Change 8:1607871.
doi: 10.3389/ffgc.2025.1607871

Vertical distribution and factors influencing tropical forest soil magnetic susceptibility in Xishuangbanna, Southwest China

Xiaoling Zhang[1,2,3], Haidong Wang[1,4]*, Hongzhan Liu[1,5], Haixia Li[1,2,3]*, Yucheng Shi[1], Guangyu Zheng[1], Fengrui Li[1], Daxiang Liu[1], Xiaoping Jiang[6], Erhui Ren[1] and Gangqiang Li[1]

[1]Faculty of Land Resources Engineering, Kunming University of Science and Technology, Kunming, China, [2]Key Laboratory of Geohazard Forecast and Geoecological Restoration in Plateau Mountainous Areas, Ministry of Natural Resources of the People's Republic of China, Kunming, China, [3]Key Laboratory of Geological Hazard Prediction and Early Warning and Ecological Protection and Restoration in the Plateau Mountainous Areas of Yunnan Province, Kunming, China, [4]Laiyang City Natural Resources and Planning Bureau, Yantai, China, [5]Yunnan Geology and Mining Engineering Survey Group Co., Ltd, Kunming, China, [6]Geological Exploration Institute of Shandong Zhengyuan, Jinan, China

Introduction: The measurement of soil magnetic susceptibility is rapid, nondestructive, and highly sensitive and has, therefore, been widely applied in soil research. In soil systems, the relationship between environmental factors and magnetic susceptibility is complex and interferes with the interpretation of magnetic susceptibility data. Therefore, clarifying the effects of soil factors on magnetic susceptibility and their mechanisms is necessary to explain changes in magnetic susceptibility. Magnetic characterization of tropical forest soils, which is primarily indicative of the climate, has been relatively poorly studied. Therefore, the magnetic characteristics of tropical forest soils and their correlations with soil physical and chemical properties must be systematically studied. Here, we describe a tropical rainforest soil profile that has not been disturbed by human activities and its patterns of low-frequency magnetic susceptibility (χ_{lf}), frequency-dependent magnetic susceptibility ($\chi_{fd}\%$), and susceptibility of anhysteretic remanent magnetization (χ_{ARM}).

Methods: Soil sampling was conducted in six plots in Xishuangbanna, China. Soil profiles were explored in 11 layers, and various soil properties were measured. Magnetic susceptibility was assessed using susceptometry, and structural equation modeling was used to analyze the relationships between soil factors and magnetic susceptibility.

Results: In all profiles, the values of χ_{lf} and χ_{ARM} increased with depth from 0 to 30 cm, decreased with depth from 30 to 80 cm, and tended to stabilize below 80 cm. $\chi_{fd}\%$ values increased with depth from 0 to 80 cm and decreased with depth below 80 cm, with particularly rapid attenuation at the bottom of the F1 and F6 profiles. Soil properties were determined, including bulk density, water content, electrical conductivity (EC), soil particle size, soil organic carbon (SOC), pH, free iron (Fe_d), poorly crystalline iron (Fe_o), total iron (Fe_t), total nitrogen (TN), and the primary chemical elements P, S, K, Si, Al, Mn, Mg, and Zr. Linear regression and structural equation modeling were used to explore the relationships between soil factors and χ_{lf}, to identify the main factors influencing the vertical distribution of soil χ_{lf}, and to analyze the processes and mechanisms by which various factors affect χ_{lf}. The results showed that the positive influence path followed EC → SOC → TN → Fe_o → χ_{lf}, and the negative influence path followed pH → N → Fe_o → χ_{lf}. Fe_o was the most important factor that directly affects χ_{lf} (β = 0.952). The ferrihydrite in Fe_o forms fine-grained magnetite and maghemite via the aging process, which is the main mechanism for increasing χ_{lf} in the 0–80-cm layer in this area. TN had an important effect on χ_{lf} because it affects Fe_o (β = 0.85).

Discussion: SOC, pH, and EC indirectly affect χ_{lf} by promoting the conversion of ferrihydrite and silicate-bound iron to Fe_o. This study highlights the role of forest soils in storing SOC and nutrients, contributing to the ecological management of forest soils.

KEYWORDS

forest soil, magnetic susceptibility, influencing factors, Xishuangbanna, structural equation modeling

1 Introduction

Soil magnetic parameters reflect a variety of characteristics, including soil formation processes, soil properties, environmental changes, and vegetation replacement. To date, these measurements have been applied in various fields (Mullins, 1977; Liu C. C. et al., 2012; Liu Q. S. et al., 2012), such as soil development in loess (Górka-Kostrubiec et al., 2016) and tropical volcanic soils (Su et al., 2015; Kirana et al., 2024b), forest soil (Manna et al., 2018; Magiera et al., 2019) and cropland slope erosion (Zhang et al., 2023), potential landslide area identification (Kirana et al., 2024a; Ramdhani et al., 2016), soil pollution by potentially toxic elements (Wang et al., 2018; Kanu et al., 2023; Putri et al., 2024; Sudarningsih et al., 2023, 2024), and paleoclimate implications of loessic soils (Maher et al., 2003; Ayoubi et al., 2019).

Among the various magnetic parameters, low-frequency magnetic susceptibility (χ_{lf}) is the most widely used because of its ease of measurement and high precision. The magnitude of soil χ_{lf} depends mainly on the type and content of magnetic minerals in the soil (Liu C. C. et al., 2012; Liu Q. S. et al., 2012; Taylor et al., 1987). The magnetic susceptibility of soils derived from igneous rocks is often lower than that of the parent material. The ferrimagnetic matter in the base horizons of the soil is inherited from primary coarse-grained rocks. The ferrimagnetic material in the upper soil horizons originates from the formation of new pedogenic superparamagnetic (SP) and stable single-domain (SSD) grains in both igneous and clastic rocks (Lu, 2000; Jordanova et al., 2016; Preetz et al., 2017). Magnetic minerals originate from three sources: primary magnetic minerals, inherited from the parent rock; secondary magnetic minerals, formed during soil formation; and exogenous magnetic minerals, introduced through human activities (Dearing et al., 1996; Liu C. C. et al., 2012; Liu Q. S. et al., 2012). The main magnetic minerals present in soil include magnetite, maghemite, hematite, goethite, lepidocrocite, and ferrihydrite. Maghemite and magnetite are ferrimagnetic minerals, whereas hematite and goethite are incomplete antiferromagnetic minerals (Maher, 1998). The relative contents and grain sizes of these two mineral classes determine the magnetic properties of the soil.

The formation and transformation of magnetic minerals in soil are affected by numerous factors, including parent material, climate, and soil environmental characteristics (Blundell et al., 2009). The magnetic background of the soil and materials that form secondary ferromagnetic minerals in the soil is determined by the parent material (Lu, 2000). A significant correlation exists between the χ_{lf} of soil and that of the parent rock (Lu, 2000; Sarmast et al., 2017; Jordanova et al., 2016; Preetz et al., 2017). At a large scale, soil χ_{lf} is affected by the distribution of climatic zones. Land use and vegetation types affect soil χ_{lf} at smaller scales (Lizaga et al., 2019; Sadiki et al., 2009; Rahimi et al., 2013). Soil environmental factors, such as soil texture, organic matter, nutrients, pH, redox conditions, and soil drainage, also affect local soil magnetic properties (Wang et al., 2008; Blundell et al., 2009; Ayoubi et al., 2014; Asgari et al., 2018).

Soil physical and chemical properties are central to soil ecology, encompassing studies on soil formation, pollution, and erosion, which collectively reflect the development and evolution of soils in different environments. Liu Q. S. et al. (2012) and Mullins (1977) reviewed the applications and factors influencing magnetic susceptibility. Studies on the relationship between soil magnetism and geochemical indicators have focused on large regions, temperate arid regions, and loess areas (Camargo et al., 2016; Jordanova et al., 2016; Quijano et al., 2014) or on soils formed from highly magnetized parent materials (e.g., basalt and gabbro) (César de Mello et al., 2020; Grison et al., 2016). Blundell et al. (2009) explored the main factors influencing magnetic susceptibility in England and Wales, identifying parent material and drainage as primary determinants. A second group of factors, including climate, relief, organic carbon, and pH, also played a significant role. Soil magnetic susceptibility in the arid regions of Iran is mainly influenced by parent material and topography, is negatively correlated with soil organic carbon (SOC) and electrical conductivity (EC), and has no significant relationship with pH (Ayoubi et al., 2014; Ayoubi and Mirsaidi, 2019; Owliaie and Ghiri, 2018). In the loess of Hungary, magnetic susceptibility is significantly positively correlated with Al, Si, Ti, Fe, Rb, Zr, SOC, sand, and clay and significantly negatively correlated with K, Ca, Sr., Ur, and $CaCO_3$ (Profe et al., 2018). Conversely, in temperate grasslands in North China, χ_{lf} is positively correlated with SOC, clay, and silt and negatively correlated with sand, indicating that magnetic susceptibility can quantitatively characterize soil erosion rates (Liu et al., 2018). In addition, χ_{lf} is negatively correlated with Si, and the accumulation of SOC inhibits Fe and Al crystallization (Borggaard, 1985; Poggere et al., 2018).

The tidal hydrologic regime could decrease the contents of soil iron oxides [i.e., total iron (Fe_t), free iron (Fe_d), and poorly crystalline iron (Fe_o)] and their ratios (Fe_o/Fe_d, Fe_d/Fe_t). Iron oxides and their ratios positively correlate with redox potential, organic matter, and nutrients and negatively correlate with soil pH (Liu et al., 2023). Iron forms coordination complexes with the O-, S-, and N-containing functional groups of organic matter (Bhattacharyya et al., 2018). Anthropogenic inputs have focused on the positive correlation between soil magnetic susceptibility and heavy metals, using magnetic susceptibility to predict the heavy metal pollution loading index (Delbecque et al., 2022; Karimi et al., 2017; Pérez et al., 2014). The magnetic properties of tropical forest soils are affected by the climate (temperature, rainfall), topography, and parent material, and magnetic susceptibility is used to characterize the climate, especially rainfall (César de Mello et al., 2020; Liu C. C. et al., 2012; Lu, 2000). However, a gap exists in literature on the distribution of forest soil magnetic susceptibility and its influencing factors in tropical regions, which needs to be systematically studied.

The relationships between various soil factors and χ_{lf} are complicated, with different regions and soil types showing different patterns, causing uncertainty in interpreting magnetic parameters. Therefore, understanding the relationships between soil χ_{lf} and the physical and chemical characteristics of the study area is necessary before using magnetic survey technology to investigate soil problems (Sarmast et al., 2017; Ayoubi et al., 2019). In this study, we selected soil profiles from weakly magnetic parent material in the tropical rainforest region of southwest China. The area features primitive forest vegetation adjacent to organic tea plantations, with no industrial or mining activities within tens of kilometers. As a result, these soil profiles remain unaffected by human disturbance, allowing us to investigate the vertical distribution of χ_{lf} and its relationship with soil environmental factors. Structural equation modeling (SEM) was used to evaluate the contribution rate and influence of soil factors on χ_{lf}, and the underlying mechanisms are discussed.

2 Materials and methods

2.1 Study area

The study area was Xishaungbanna (22°21′N, 100°55′E) (Figure 1) in Yunnan Province, China. The Xishuangbanna tropical rainforest spans three counties—Jinghong, Menghai, and Mengla—and is the largest and most intact tropical rainforest in China, with 85.8% of its area covered by forest. Numerous species, including *Terminalia myriocarpa, Myristica yunnanensis, Horsfieldia tetratepala*, and *Homalium laoticum* have been identified in the region. The terrain slopes from east to west, with elevations ranging from 688 to 1,797.3 m. The regional hydrology is dominated by surface water. Located south of the Tropic of Cancer, the region experiences a northern tropical humid monsoon climate with rainy (May to October) and dry (November to April) seasons. The annual average temperature is approximately 18°C, the annual average sunshine duration is approximately 2,000 h, and the annual average rainfall is 1,200–1,700 mm.

2.2 Soil sampling

In the study area, six plots with different slopes, slope directions, and elevations were established and designated F1–F6 (Figure 1). The soil type is Ferralsols, and the parent rock is Mesozoic Lower Cretaceous purple-red siltstone and mudstone. First, plant residue, roots, stones, and apparent macrofauna were manually removed. A pit was then dug with approximate dimensions of 80 cm in width, 100 cm in length, and ≥140 cm in depth. Soil profiles were explored in 11 layers (0–10, 10–20, 20–30, 30–40, 40–50, 50–60, 60–70, 70–80, 80–100, 100–120, and 120–140 cm). A wooden shovel was used to collect soil samples to avoid disturbing their magnetic properties. The bulk density (BD) and water content (WC) of the soil samples were measured using a soil core sampler (volume, 100 cm^3). Next, the soil samples were placed in individually labeled aluminum boxes of known weight (M_0), weighed to determine fresh weight (M_1, i.e., the soil sample plus M_0), and brought back to the laboratory.

2.3 Measurements

2.3.1 Magnetic properties

χ_{lf} was measured using an AGICO MFK1 FA susceptometer (AGICO, Brno, Czech Republic) at frequencies of 976 (hereafter χ_{lf})

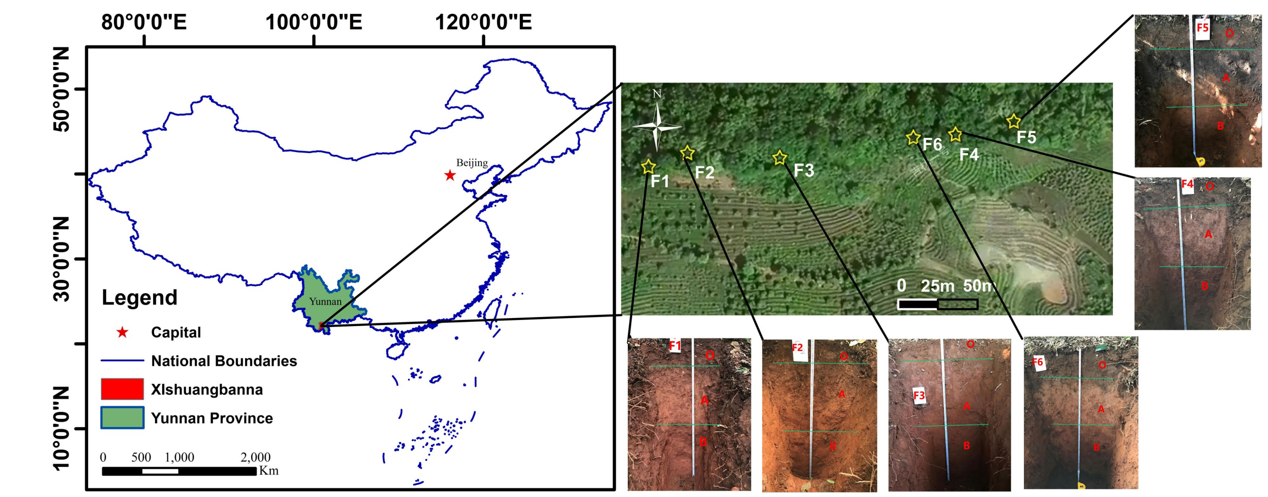

FIGURE 1
Study area and soil sampling locations in Yunnan Province, southwest China (soil profile, O. humus layer, greyish black, loose, plant debris; A. leachate, Reddish brown, sandy loam; B. alluvium, Reddish brown, sandy loam;). The satellite imagery was obtained from the OweMap (Ovi Map) Windows Client v10.1.8, and the website is https://www.ovital.com.

and 1,561 (hereafter χ_{hf}) Hz. From these measurements, frequency-dependent magnetic susceptibility (χ_{fd}) was calculated as $(\chi_{lf} - \chi_{hf}) \times \ln 10/[(\ln(f_{mHf}) - \ln(f_{mLf})]$ (Hrouda, 2011). Relative frequency-dependent magnetic susceptibility (χ_{fd}%) was calculated as $100 \times (\chi_{lf} - \chi_{hf}) \times \ln 10/[(\ln(f_{mHf}) - \ln(f_{mLf}) \times (\chi_{lf})]$ (Hrouda, 2011). Here, f_{mHf} is the high frequency (1,516 Hz), and f_{mLf} is the low frequency (976 Hz). Therefore, χ_{fd} and χ_{fd}% were obtained after conversion based on measurement data. Anhysteretic remanent magnetization (ARM) was induced using a peak alternating field of 100 mT and a constant biasing field of 0.05 mT. This parameter is expressed as χ_{ARM} after normalization. Information related to the magnetic parameters used in the experimental method is presented in Table 1.

2.3.2 Soil physicochemical properties

Soil pH was determined using a glass electrode (soil: H_2O = 1:2.5). SOC was determined using the potassium dichromate oxidation method. EC was measured using an electrical conductivity meter. Soil particle size distribution was determined using the laser diffraction method with a laser particle sizer, and the soil was divided into silt, sand, and clay. The aluminum box (of mass M_0, including the 100-cm^3 sample collected using a ring cutter) was placed in an oven at 105 ± 2°C for 8 h, and the volumes M_1 and M_2 were recorded before and after drying, respectively. WC and BD were determined using Equations 1, 2, respectively.

$$WC(\%) = (M_1 - M_2)/(M_2 - M_0) \times 100 \quad (1)$$

$$BD(g/cm^3) = (M_2 - M_0)/100 \quad (2)$$

Information related to the physicochemical properties of the soil used in the experiments is presented in Table 1.

TABLE 1 Maximum and minimum values of the soil magnetic parameter and physiochemical properties of the six profiles.

Variable	Profile											
	F1		F2		F3		F4		F5		F6	
Slope aspect (°)	NW325°		NW332°		SE172°		NW315°		NW311°		NE28°	
Slope angle (°)	20°		15°		19°		23°		29°		18°	
Elevation (m)	1,348		1,346		1,350		1,345		1,334		1,338	
	Mix	Min	Mix	Min	Mix	Min	Mix	Min	Mix	Min	Mix	Min
χ_{lf} (10^{-8} m^3/kg)	183.15	16.42	211.87	29.34	185.06	28.83	153.86	12.38	223.55	16.18	103.56	6.33
χ_{fd} (10-^{8} m^3/kg)	25.256	1.22	29.64	3.45	29.52	3.72	21.58	1.13	31.3	1.43	14.49	0.12
χ_{fd} (%)	8.68	4.51	9.02	7.35	10.28	8.06	8.89	5.69	8.75	5.51	8.75	1.17
χ_{ARM} (10^{-8} m^3/kg)	863.55	60.99	1126.41	135.34	1172.54	166.82	589.50	53.68	907.04	62.25	436.28	13.53
Fe_t (g/kg)	61.21	33.17	–	–	36.24	29.08	39.60	30.27	–	–	41.86	22.13
Fe_o (g/kg)	7.07	2.09	–	–	2.34	1.60	5.63	1.40	–	–	4.78	1.91
Fe_d-Fe_o (g/kg)	38.55	15.78	–	–	25.51	17.85	26.28	15.90	–	–	27.98	9.97
Fe_t-Fe_d (g/kg)	20.57	10.32	–	–	10.27	7.29	12.20	9.08	–	–	11.58	8.55
WC (%)	34.47	29.98	49.98	32.39	24.08	20.31	32.13	27.7	40.34	33.41	30.03	23.13
BD (g/cm^3)	1.4	1.2	1.34	0.7	1.45	0.91	1.48	0.82	1.27	0.91	1.48	1
EC (%)	60.65	38.05	66.75	35.8	45.05	22.7	63.2	31.6	67.85	27	53.4	37.05
Clay (%)	18.81	10.59	19.79	14.29	19.78	13.87	17.11	13.8	–	–	–	–
Slit (%)	76.13	65.54	73.16	61.89	72.07	62.24	69.46	61.29	–	–	–	–
Sand (%)	19.41	9.8	21.23	10.1	20.66	9.05	21.84	15.69	–	–	–	–
pH	4.54	4.24	4.61	4.21	4.86	4.35	4.52	4	4.81	4.25	4.66	4.42
SOC (g/kg)	28.27	4.76	35.33	6.4	27.43	2.68	34.48	3.23	30.86	4.1	25.84	3.42
TN (g/kg)	2.33	0.61	–	–	1.5	0.3	2.39	0.29	–	–	1.38	0.41
P (%)	0.038	0.024	–	–	0.043	0.021	0.044	0.017	–	–	–	–
K (%)	1.74	1.3	–	–	0.75	0.55	1.42	1.12	–	–	–	–
S (%)	0.027	0.005	–	–	0.025	0.008	0.027	0.005	–	–	–	–
Si (%)	25.34	21.04	–	–	28.59	24.44	27.28	24.63	–	–	–	–
Al (%)	12.58	10.28	–	–	11.27	8.87	11.47	9	–	–	–	–
Mg (%)	0.87	0.66	–	–	0.52	0.41	0.78	0.59	–	–	–	–
Mn (%)	0.014	0.006	–	–	0.013	0.006	0.019	0.006	–	–	–	–
Zn (%)	0.014	0.006	–	–	0.013	0.006	0.019	0.006	–	–	–	–

2.3.3 Determination of soil elements and Fe oxides

We selected four soil profiles—F1, F3, F4, and F6—to study the characteristics of the different forms of iron distribution in the soil. Fe_o was determined using acid ammonium oxalate extraction (McKeague and Day, 1966; McKeague et al., 1971). Fe_d was extracted using the citrate–bicarbonate–dithionate method (Mehra and Jackson, 1958). Fe_t in the soil was determined using the sodium carbonate melting method. Crystalline iron (Fe_c) was calculated by subtracting poorly crystalline iron from free iron ($Fe_c = Fe_d - Fe_o$) (Schwertmann, 1985, 1988), and silicate-bound iron was calculated by subtracting free iron from total iron ($Fe_r = Fe_t - Fe_d$) (Blume and Schwertmann, 1969). Total nitrogen (TN) was determined using the Kjeldahl method (Bremner and Mulvaney, 1982). The concentrations of Si, Al, P, S, K, Ca, Na, Mg, Mn, Ti, Zr, and other elements were determined using X-ray fluorescence spectroscopy. Information related to the determination of soil elements and iron oxides used in the experiment is shown in Table 1.

2.4 Data analysis

SEM is an advanced statistical method that allows for hypothesis testing of complex path–relation networks (Grace et al., 2007). The model was developed based on collected experimental datasets, excluding reverse causality through a comprehensive literature review, thereby strengthening model credibility. Initially, a missing-value test was performed on all data. Thereafter, an initial model of the factors affecting soil χ_{lf} was established based on current theoretical knowledge and the main driving factors known to cause changes in soil χ_{lf}. Next, we parameterized the initial structural equation model using a correction factor to test the goodness of fit using the chi-square test, degrees of freedom, estimated values, and the standardized root mean square residual. Finally, we used chi-square/degree of freedom < 3, probability level > 0.05, Tucker–Lewis index > 0.95, and standardized root mean square residual < 0.08 (Shi et al., 2018) to identify the optimal model for χ_{lf} in this study. Structural equation model construction was achieved using AMOS 20 (Amos Development Corporation, Meadville, PA, USA). The section and linear regression analysis results were plotted using Origin 8.0 (OriginLab, Northampton, MA, USA). One-way analysis of variance and Pearson's correlation analyses were performed using SPSS 22.0 (SPSS Inc., Chicago, IL, USA).

3 Results

3.1 Analysis of soil parameter profiles

3.1.1 Vertical distribution characteristics of χ_{lf}, χ_{fd}, and χ_{ARM}

The χ_{lf} values ranged from 6.3×10^{-8} to 190×10^{-8} m^3 kg^{-1}, with a mean value of 87.8×10^{-8} m^3 kg^{-1} (Figure 2A). The χ_{ARM} values ranged from 13.5×10^{-8} to $1,172.5 \times 10^{-8}$ m^3 kg^{-1}, with a mean value of 420.5×10^{-8} m^3 kg^{-1} (Figure 2B). The mean values of χ_{lf} and χ_{ARM} for 0–60-cm soil layers (133.4×10^{-8} and 645.9×10^{-8} m^3 kg^{-1}, respectively) were higher than those for <60-cm layers (33.1×10^{-8} and 149.9×10^{-8} m^3 kg^{-1}, respectively). In the 0–80-cm soil layer, the change in χ_{fd}% was small, within a range of 10–13.7% (Figure 2C), while the 80–140-cm soil layer showed a decreasing trend, with greater differences among the six sections, varying from 2 to 15% (Figure 2C). Overall, χ_{lf}, χ_{ARM}, and χ_{fd}% showed similar change trends with soil profile depth, increasing first and then decreasing (Figures 2A–C), similar to the change in soil magnetism in the weakly magnetic parent materials (Li et al., 2024; Torrent et al., 2010). The χ_{lf} values for profiles F2 and F5 at the foot of the lowlands were much greater than the F6 profiles at the top of the slope. The χ_{fd}% values of the soil layers above 80 cm were all >10, indicating that the χ_{lf} values were derived from SP particles (Dearing et al., 1996). The χ_{fd}% values at the bottom of the F1 and F6 profiles were 5 to 6%, respectively, indicating that the soil magnetic minerals were

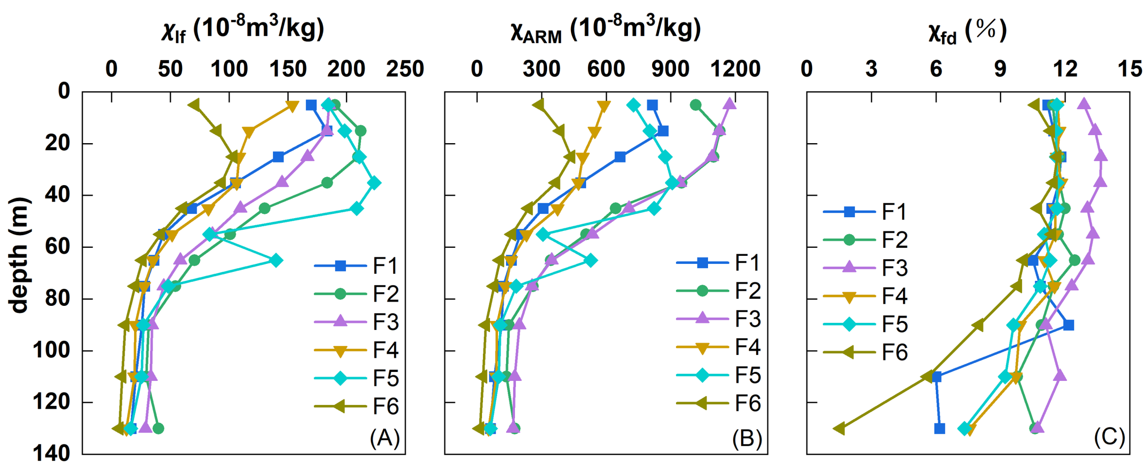

FIGURE 2
Vertical distribution of magnetic susceptibilities. **(A)** low-frequency magnetic susceptibility (χ_{lf}), **(B)** susceptibility of anhysteretic remanent magnetization (χ_{ARM}), **(C)** frequency-dependent magnetic susceptibility (χ_{fd}).

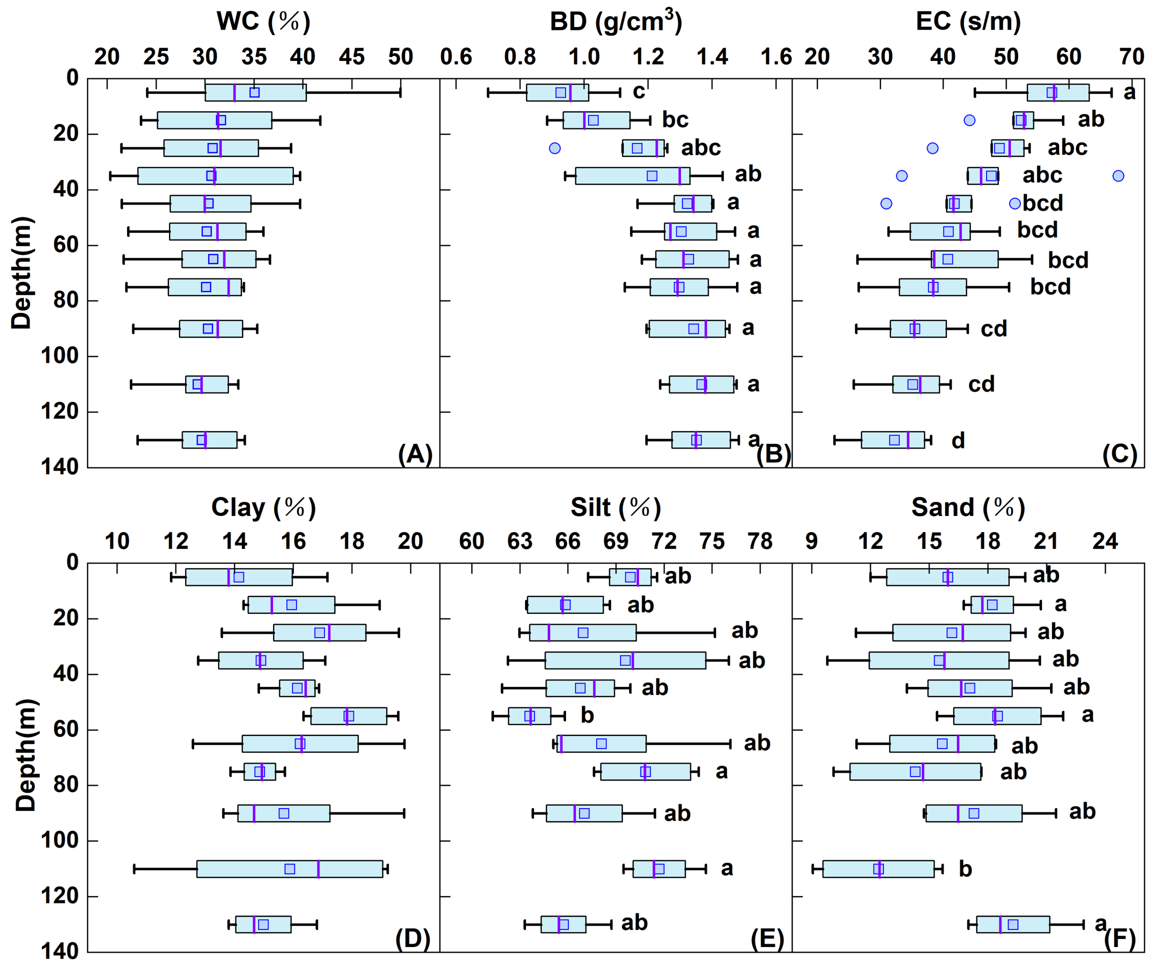

FIGURE 3
Vertical distribution of soil physical properties. **(A)** water content (WC), **(B)** bulk density (BD), **(C)** electrical conductivity(EC), **(D)** clay, **(E)** silt, **(F)** sand. (The light blue fill range represents 25 per cent to 75 per cent of the data. Purple line represents the median, boxes indicate mean values, circles indicate outliers. a,b,....Various letter means significant different at $P < 0.05$ probability level.)

dominated by coarser multidomain (MD) and pseudo-single-domain particles (PSD) (Dearing et al., 1996; Fine et al., 1993).

3.1.2 Soil physical property profiles

WC and EC decreased with increasing soil depth and then gradually stabilized (Figures 3A,C). No significant differences were observed in WC between the layers (Figure 3A). Significant differences in EC were observed at 0–10- and 50–140-cm depths ($p < 0.01$) (Figure 3C). BD increased with depth and significantly differed between the 0–20- and 50–140-cm soil layers ($p < 0.01$, Figure 3B). The percentage of soil silt was >65% in all profiles (Figure 3E). Soil clay, silt, and sand content showed no obvious trends with soil depth and small non-significant differences among the layers (Figures 3D–F).

3.1.3 Soil chemical property profiles

SOC, TN, P, S, Si, Mn, and Zr contents decreased with increasing soil depth and then gradually stabilized (Figures 4A,C,D,F,G,J,K). The differences in SOC content among the soil layers were significant. The TN, P, and S contents differed significantly between the 0–10- and 30–140-cm layers ($p < 0.01$) (Figures 4C,D,F). No significant differences in K, Si, Mg, and Mn contents were observed among the layers ($p > 0.05$) (Figures 4E,G,I). The pH, as well as Al and Mg contents, increased with soil depth, but the changes were small (Figures 4B,H,I). The pH values differed significantly between the 0–60- and 140-cm soil layers ($p < 0.01$) (Figure 4B). The Al content significantly differed between the 0–10- and 80–140-cm layers ($p < 0.05$) (Figure 4H).

3.1.4 Soil iron oxide profiles

Fe_t, Fe_c, and Fe_r gradually increased with soil depth (Figure 5A,C,D). Fe_t values differed significantly between the 0–30- and 100–120-cm soil layers ($p < 0.01$), as did the Fe_c values between the 0–10- and 120–140-cm layers ($p < 0.01$). However, Fe_r did not differ significantly among the layers ($p > 0.01$). Fe_o gradually decreased with increasing soil depth, consistent with the distribution characteristics of soils with the same parent material in the Sichuan Basin (Figure 5B) (Huang et al., 2024). Fe_o values in the surface layer (0–20 cm) were significantly higher than those in the 80–140-cm layer ($p < 0.01$).

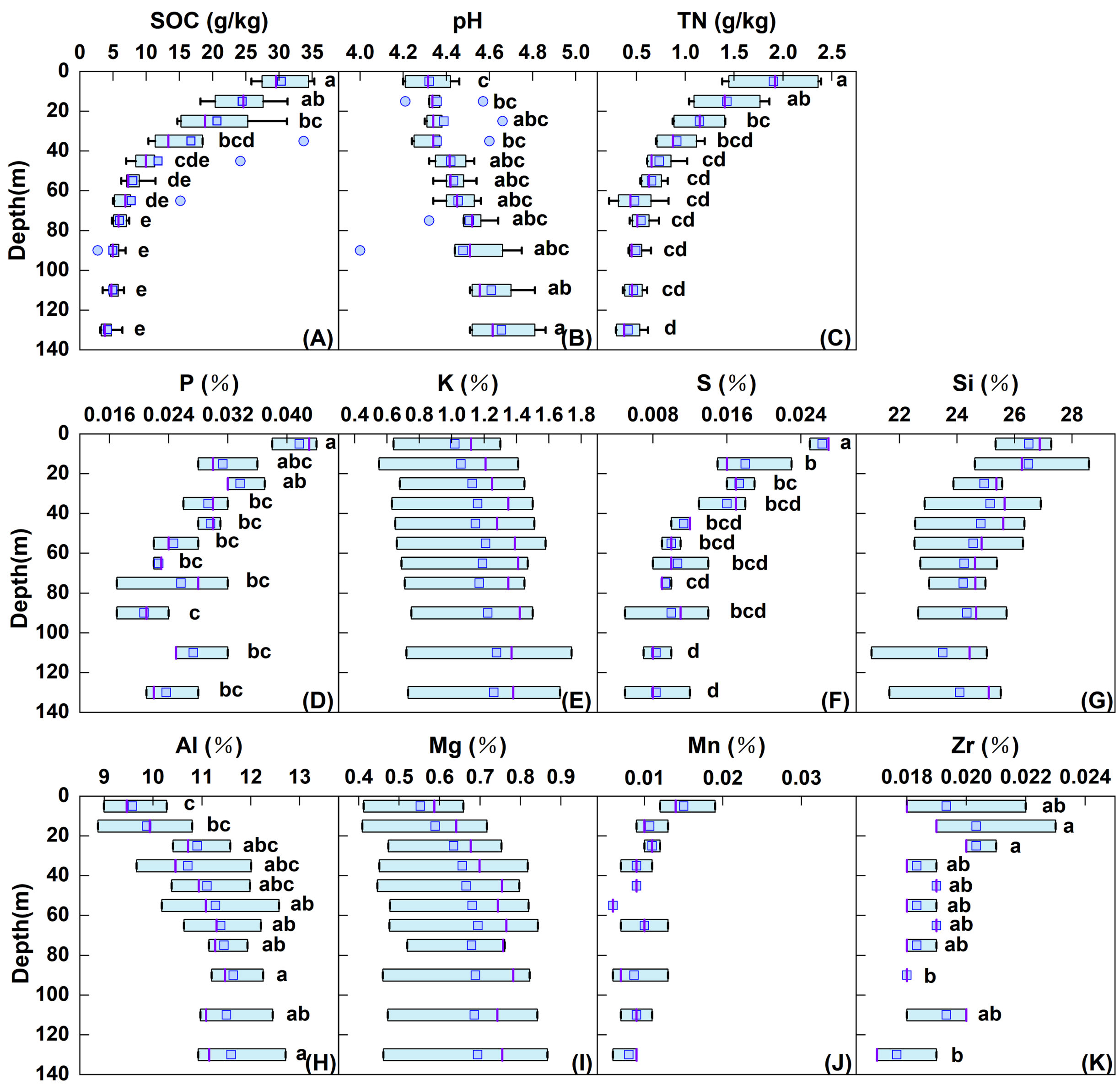

FIGURE 4
Vertical distribution of soil chemical properties. **(A)** total soil organic carbon (SOC), **(B)** pH, **(C)** total nitrogen (TN), **(D)** phosphorus (P), **(E)** potassium (K), **(F)** sulfur (S), **(G)** silicon (Si), **(H)** aluminum (Al), **(I)** magnesium (Mg), **(J)** manganese (Mn), **(K)** zirconium(Zr). (The light blue fill range represents 25 per cent to 75 per cent of the data. Purple line represents the median, boxes indicate mean values, circles indicate outliers. a,b,....Various letter means significant different at $P < 0.05$ probability level.)

3.2 Correlations between χ_{lf} and soil parameters

3.2.1 Correlations between χ_{lf} and soil physical parameters

χ_{lf} was positively correlated with EC and WC ($p < 0.01$, Figures 6A,B) and negatively correlated with BD ($p < 0.01$, Figure 6C). No correlations were observed between χ_{lf} and clay, silt, or sand ($p > 0.05$, Figures 6D–F).

3.2.2 Correlations between χ_{lf} and soil chemical parameters

χ_{lf} was positively correlated with SOC, S, TN, TP, Si, Mn, and Zr ($p < 0.01$, Figures 7A–G) but negatively correlated with pH and Al ($p < 0.01$, Figures 7H,I) and with Mg and K ($p < 0.05$, Figures 7J,K).

3.2.3 Correlations between χ_{lf} and Fe oxides

χ_{lf} was positively correlated with Fe_o ($p < 0.01$, Figure 8A) but negatively correlated with Fe_t and Fe_c ($p < 0.01$, Figures 8B,C) and with Fe_r ($p < 0.05$, Figure 8D).

4 Discussion

4.1 Pathways and contributions of factors affecting χ_{lf}

According to the linear regression analysis, the factors with potentially positive effects on χ_{lf} included Fe_o, EC, SOC, TN, P, S, Si, Mn, and Zr, and those with potentially negative effects were Fe_t, Fe_r, Fe_c, BD, pH, Al, Mg, and K. We identified important factors for a

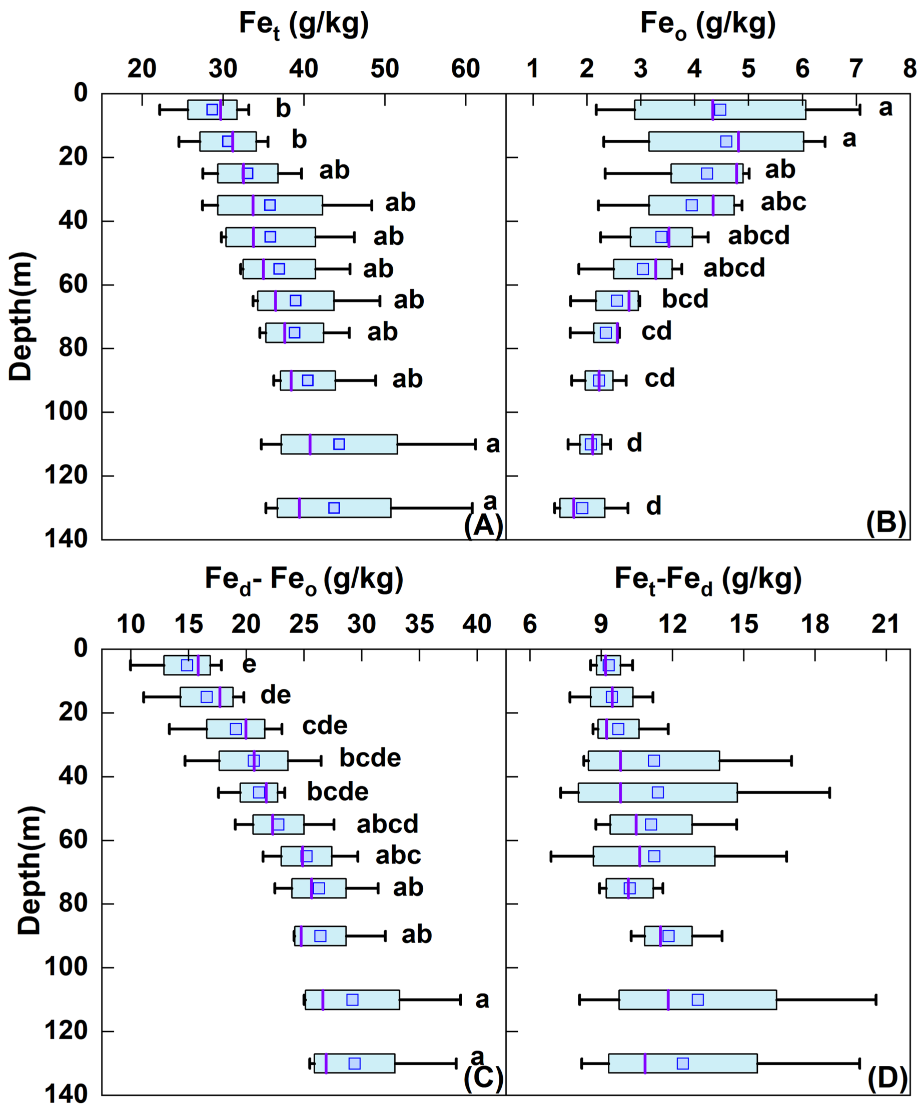

FIGURE 5
Vertical distribution of soil iron oxide. **(A)** total iron (Fe_t), **(B)** poorly crystalline iron (Fe_o), **(C)** crystalline iron (Fe_d - Fe_o), **(D)** silicate-bound iron (Fet - Fed). (The light blue fill range represents 25 per cent to 75 per cent of the data. Purple line represents the median, boxes indicate mean values, circles indicate outliers. a,b,....Various letter means significant different at $P < 0.05$ probability level.).

comprehensive structural equation model of the main pathways and the contribution rates of each factor affecting χ_{lf}.

The types and relative contents of iron oxides present in the soil are direct drivers of χ_{lf}, and soil environmental factors indirectly affect χ_{lf} by affecting the conversion of iron oxides. We used Fe_o, Fe_c, and Fe_r as the iron oxide (or iron hydroxide) types and EC, pH, SOC, TN, P, and S as the environmental factors for the structural equation model fitting analysis. Studies have shown that these six soil environmental factors are closely related to the formation and alteration of magnetic minerals in soil (Blundell et al., 2009; Ayoubi et al., 2014; Melton et al., 2014; Bhattacharyya et al., 2018; Ji et al., 2019). Based on their vertical trends, χ_{lf}, SOC, TN, S, and EC also showed good consistency (Figures 2C, 3A–C). Therefore, other factors were not used for structural equation model fitting. Fe_t is the sum of Fe_o, Fe_r, and Fe_c and does not contribute to model fitting. Soil Si exists mainly in the form of diamagnetic minerals, which reduce the magnetic susceptibility of the soil (Rochette, 1987; Jörn et al., 2018). The main processes driving soil development are desilication and modification with aluminum-rich iron. The leaching and deposition of Fe_t and Al tend to increase from the surface layer downward, whereas that of Si decreases gradually (Wang et al., 2013). In the present study, χ_{lf} was positively correlated with Si and negatively correlated with Fe_t and Al (Figures 7E,I, 8B), which may be due to the soil formation process noted above. Mn and iron oxides form nodules in the soil (Gasparatos et al., 2019), and Zr is a relatively stable element in the soil (Faměra et al., 2018). Moreover, the differences in Si and Mn values in the study area were not significant (Figure 4G). In addition, Zr does not correspond to magnetic parameters in the profile, with no relevant literature on its relationship with soil magnetism. Therefore, these parameters were not considered major factors affecting the vertical distribution characteristics of χ_{lf} and were not considered in model fitting. Salts containing K and Mg in the soil are diamagnetic substances (Ayoubi et al., 2014), and K and Mg were negatively correlated with χ_{lf} (Figures 7J,K). However, the correlation between χ_{lf},

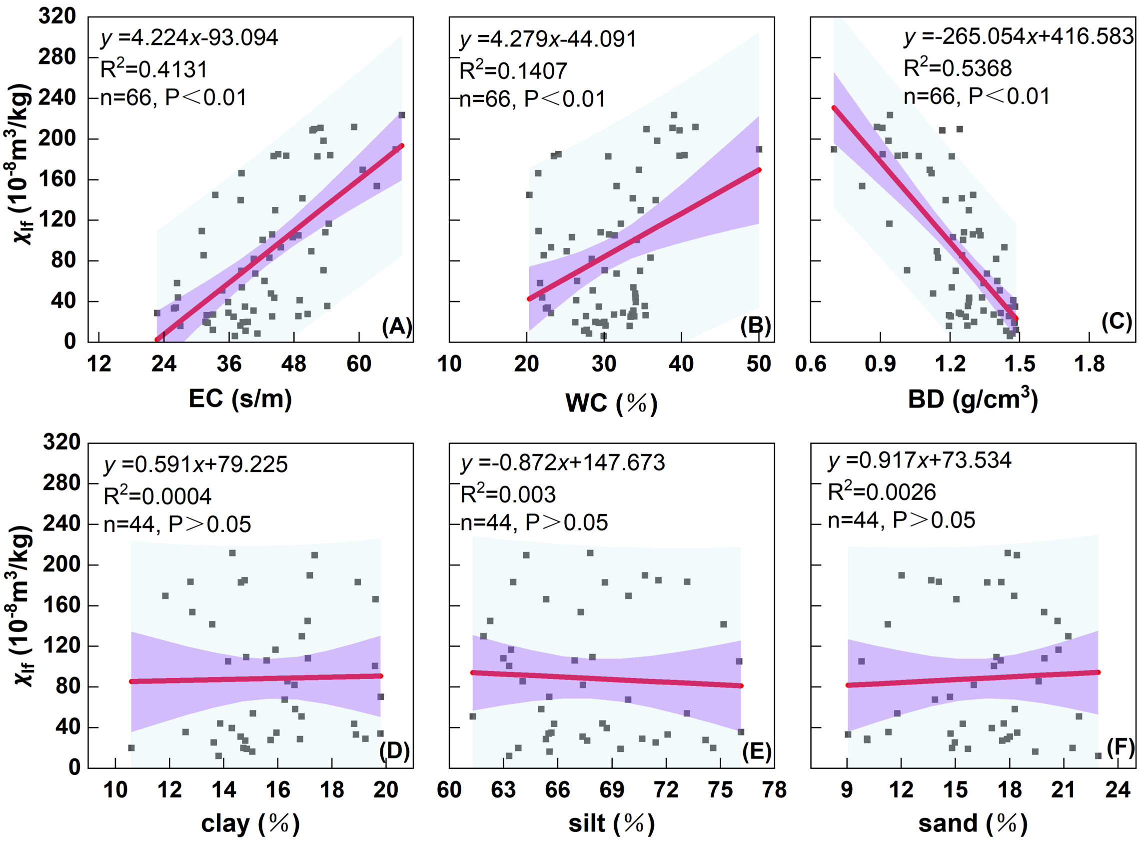

FIGURE 6
Relationships between χ_{lf} and **(A)** EC, **(B)** WC, and **(C)** BD, **(D)** clay, **(E)** silt, **(F)** sand.

K, and Mg in the current study was relatively weak, and EC primarily reflected the influence of soluble salts. Therefore, EC was used as a factor for model construction, and Mg and K were not considered in the model fitting. χ_{lf} was significantly and negatively correlated with BD, which is a comprehensive indicator of soil minerals, organic matter, pores, and other factors (Ayoubi et al., 2019), making the results difficult to interpret. In this case, BD was also negatively correlated with SOC; therefore, SOC was used as a factor, and BD was excluded from model fitting.

The initial model was constructed based on the correlations among the factors from previous research results (Table 2). P and S contents were eliminated during model optimization. These factors were linearly related to χ_{lf} (Figures 7B,D); however, these correlations may be due to the adsorption of iron oxides onto these two elements (Ajmal et al., 2018; Johnston et al., 2016; Marques et al., 2014). Moreover, P and S were significantly correlated with SOC (Table 2) and TN (Table 2). Relationships exist based on the binding or direct interactions between P, S, SOC, and TN (Li et al., 2012). EC significantly promoted SOC accumulation, exhibiting a strong positive correlation ($r = 0.82$). In turn, it drives an increase in TN content with an extremely high positive correlation ($r = 0.93$). TN further facilitated the formation of Fe_o, which exhibited a robust positive correlation ($r = 0.87$). Conversely, elevated soil pH levels reduce Fe_o formation, displaying a moderate negative correlation ($r = -0.52$). Based on these results, combined with findings from literature, the final model included SOC and TN, whereas P and S were eliminated (Figure 9). The significance level of the model was <0.05, indicating good agreement between the model and observed data.

The final model fitting results showed a positive influence path in the order of EC → SOC → TN → Fe_o → χ_{lf} and a negative influence path in the order of pH → N → Feo → χ_{lf}. The direct path effect of Fe_o on χ_{lf} was significant ($\beta = 0.952$), with Fe_o identified as the primary factor affecting χ_{lf}. Compared with the same parent material soil in southwest China, the χ_{lf} value of Xishuangbanna soil was 10-fold higher than that of Sichuan Basin soil, which was mainly due to the fact that the Fe_o content of Xishuangbanna soil ($Fe_{o\ max} = 7.07$ g/kg) was 2-fold higher than that of Sichuan Basin soil ($Fe_{o\ max} = 3.4$ g/kg) (Huang et al., 2024). EC, SOC, TN, and pH affected χ_{lf} by influencing Fe_o or by promoting the conversion of Fe_c and Fe_r to Fe_o. TN exhibited a direct positive impact on Fe_o ($\beta = 0.853$). Studies have shown that the chemodenitrification of nitrogen and microbial NO_3-dependent Fe(II) oxidation in the soil can produce Fe_o (Li et al., 2018a). SOC had a negative impact on both Fe_c ($\beta = -0.771$) and Fe_r ($\beta = -0.435$). Organic carbon is an important factor in the transformation of Fe_c to Fe_o (Lindsay, 1991; Colombo et al., 2014; Calabrese and Porporato, 2019). The combined action of organic matter and water promotes the weathering of Fe_r to release iron, which forms active iron by interacting with water (Calabrese and Porporato, 2019). Iron oxides in the soil adsorb organic carbon and form coprecipitates, which can hinder the crystal aging process of Fe_o (Pizarro et al., 2003; Xu et al., 2019). pH has a negative direct path effect on Fe_c ($\beta = -0.243$), with lower pH promoting the reduction of Fe^{3+} to Fe^{2+}. pH also indirectly affects χ_{lf}

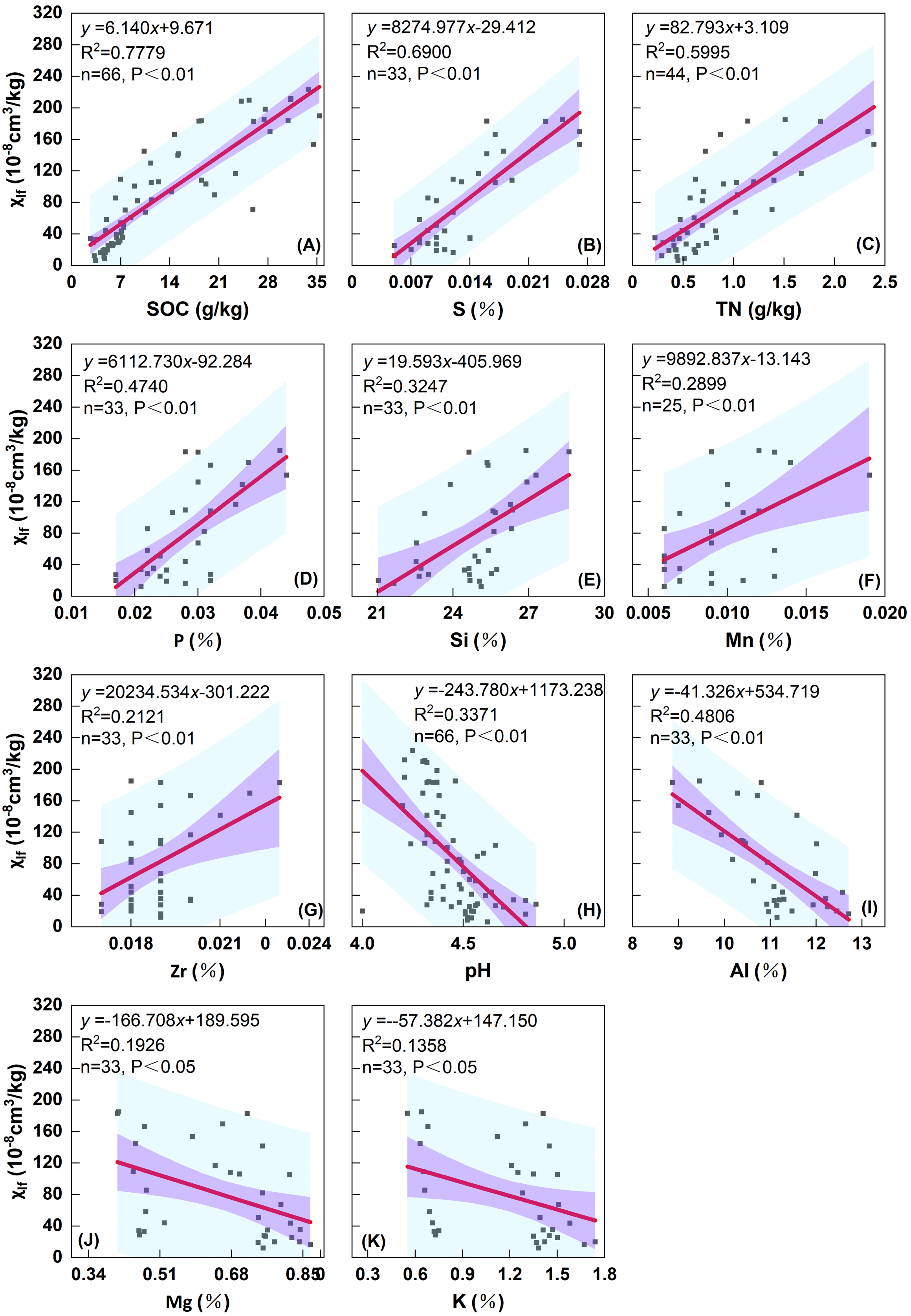

FIGURE 7
Relationships between χ_{lf} and **(A)** SOC, **(B)** S, **(C)** TN, **(D)** P, **(E)** Si, **(F)** Mn, **(G)** Zr, **(H)** pH, **(I)** Al, **(J)** Mg, and **(K)** K.

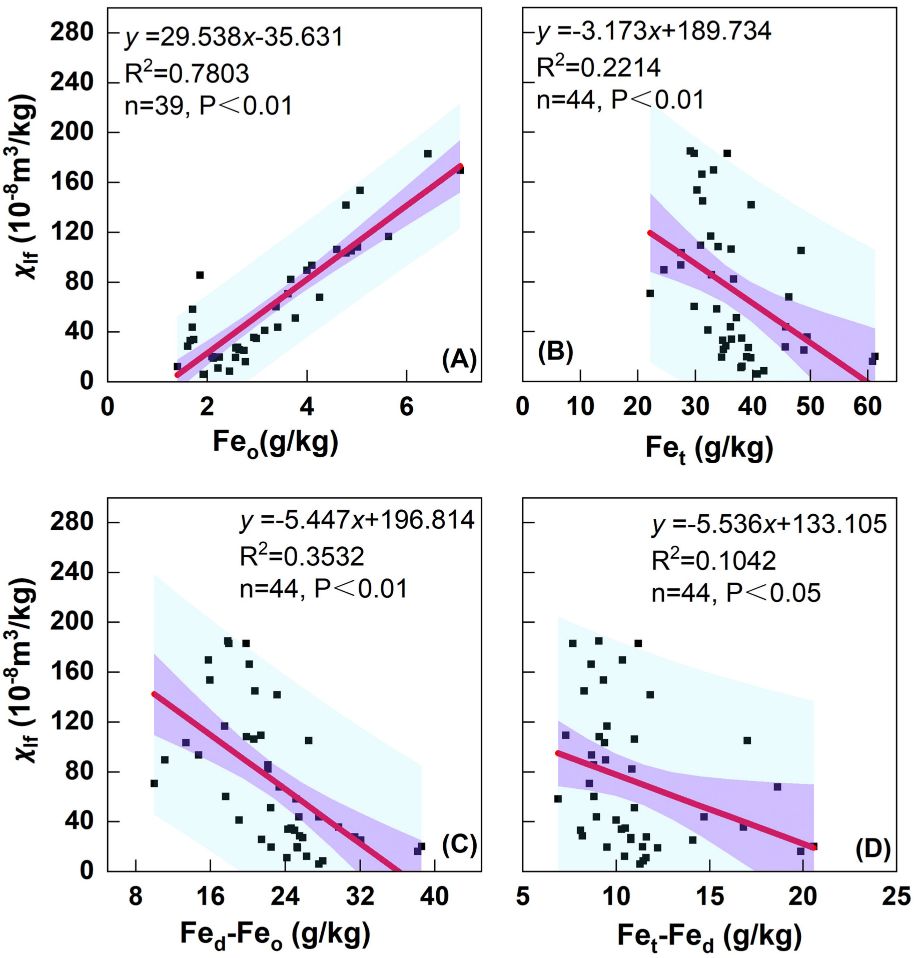

FIGURE 8
Relationships between χ_{lf} and **(A)** Fe_o, (B) Fe_t, **(C)** Fe_d - Fe_o, and **(D)** Fe_t - Fe_d.

TABLE 2 **Pearson correlation coefficients between iron oxide and soil properties in the studied area.**

	SOC	pH	TN	P	S	EC	Fe_o	Fe_d - Fe_o	Fe_t - Fe_d
SOC	1								
pH	−0.57**	1							
TN	0.93**	−0.52**	1						
P	0.8**	−0.32	0.79**	1					
S	0.9**	−0.44**	0.85**	0.72**	1				
EC	0.82**	−0.65**	0.77**	0.69**	0.64**	1			
Fe_o	0.84**	−0.38*	0.87**	0.67**	0.86**	0.72**	1		
Fe_d - Fe_o	−0.71**	−0.02	−0.48*	−0.37	−0.7**	−0.48*	−0.57**	1	
Fe_t - Fe_d	−0.37*	−0.12	−0.17	−0.06	−0.35	−0.2	−0.2	0.76**	1

SOC, soil organic carbon; pH; TN, total nitrogen; P, phosphorus; S, sulfur; EC, electrical conductivity; Feo, poorly crystalline iron; Fed - Feo, crystalline iron; Fet - Fed, silicate-bound iron.
*$P < 0.05$, **$P < 0.01$.

by altering TN. The pH of the soil system is an important factor affecting nitrification and denitrification processes, higher pH being beneficial for chemical denitrification (Zhang et al., 2011). EC positively affected SOC and indirectly affected χ_{lf} by increasing SOC accumulation. EC is a comprehensive measure of soluble salts in the soil, and high concentrations of these electrolytes decrease the susceptibility of organic matter to decomposition by microorganisms. A high concentration of Na^+ in the soil causes clay particles to flocculate into agglomerates, thereby reducing the decomposition of soil organic matter (Chen et al., 2019). Calcium ions in the soil bind to free radicals in organic matter, forming a layer of calcium carbonate on the particle surface, thereby inhibiting the decomposition of

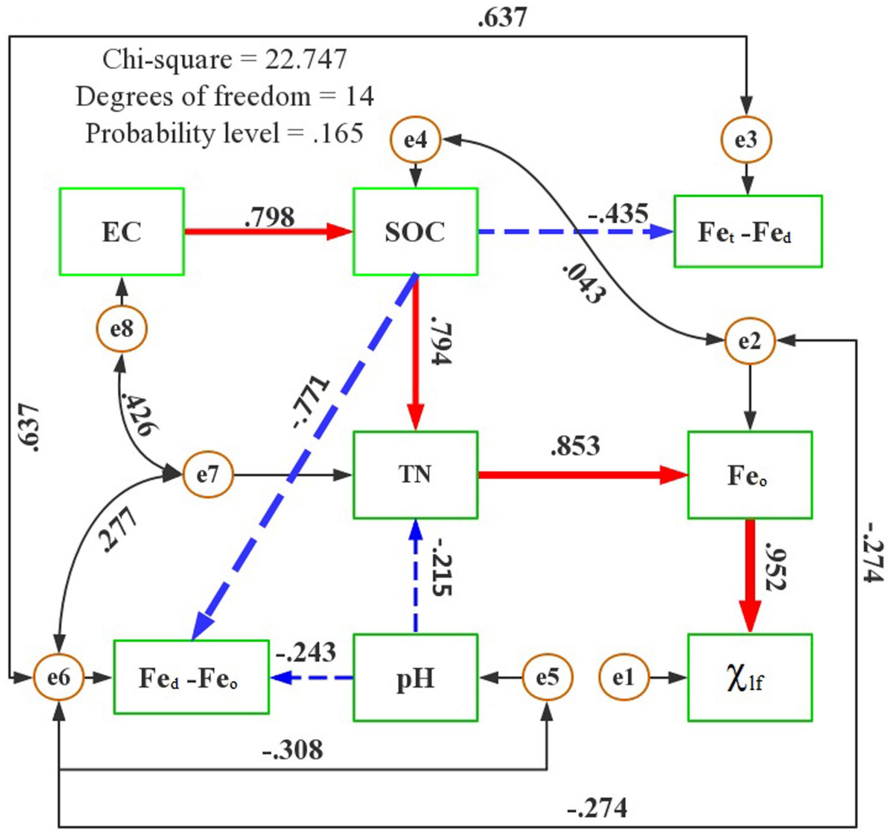

FIGURE 9
Structural equation models (SEM) results. The effects on χ_{lf} from Fe_o, Fe_d - Fe_o, Fe_t - Fe_d, EC, TN, SOC, pH. Arrow means the effect path and direction; red and blue lines mean the positive and negative effect, respectively. Numbers on arrows are standardized path coefficients($P < 0.05$). "e" means the error of input data.

organic matter (Li et al., 2018a). SOC also affects χ_{lf} by promoting the accumulation of organic nitrogen-containing microbial carbon. Microorganisms are involved in nitrogen cycling, and an increase in their content promotes nitrogen fixation (Xiao et al., 2019).

4.2 Mechanism iron oxide changes affecting χ_{lf} in soil

χ_{fd} is particularly sensitive to SP ferrous minerals (Bloemendal et al., 1985); when χ_{fd} is >10%, SP particles are abundant (Oldfield, 1991; Fine et al., 1993). In the six plots in the study area, χ_{fd} was substantially >10% in the 0–80-cm soil layer (Figure 2). χ_{ARM} is sensitive to SSD and small PSD magnetic ferrous minerals (Banerjee et al., 1981). χ_{lf} and χ_{fd}% were related exponentially, whereas χ_{lf} and χ_{ARM} were related linearly (Figures 10A,B). Our results showed that ferrimagnetic minerals in soil exist mainly as SP and single-domain particles. Fine-grained magnetic minerals were the leading cause of the increase in χ_{lf} in the 0–80-cm soil layer. Magnetic minerals present as fine particles in soil are mainly magnetite and maghemite formed during soil formation (Maher and Taylor, 1988; Preetz et al., 2017). The results of this study showed that χ_{lf} was significantly and positively correlated with Fe_o (Figure 8A), indicating that ferrimagnetic minerals in fine particles could be extracted from ammonium oxalate solutions. Fine-grained ferrimagnetic minerals are mainly found in Fe_o, and some studies have shown that χ_{lf} is positively correlated with both Fe_o and Fe_d (Lu, 2000; Hu et al., 2009; Li et al., 2017).

Combining the SEM results with those of previous studies, we determined the relationships between iron oxide conversion, soil χ_{lf} changes, and soil environmental factors. The crystal lattice of the primary silicate mineral in the soil is destroyed by weathering, and the released iron combines with water to form Fe_o. When external factors (e.g., temperature, redox conditions, organic matter, and pH) change, iron oxides are oxidized, dehydrated, and crystallized, leading to aging. Iron oxides form crystalline iron oxides during the aging process, and Fe_c can be converted to Fe_o during the activation process under certain conditions (Winkler et al., 2018).

The main component of Fe_o is ferrihydrite, which has been suggested to form magnetite and maghemite. When a high concentration of Fe^{2+} is present in a solution, ferrihydrite is dehydrated and oxidized to form magnetite because of the activity of reducing bacteria. Magnetite can be further oxidized to form maghemite (Schwertmann, 1988; Dearing et al., 1996; Pallud et al., 2010). Some researchers have proposed that maghemite forms SP particles during ferrihydrite aging. Through oxidation, the grains become larger and eventually transform into hematite (Torrent et al., 2006; Jiang et al., 2018). Fe_o increases χ_{lf} by promoting the formation of magnetite and maghemite, whereas the aging of maghemite to hematite reduces χ_{lf}. Soil environmental factors such as SOC, TN, pH, and EC significantly

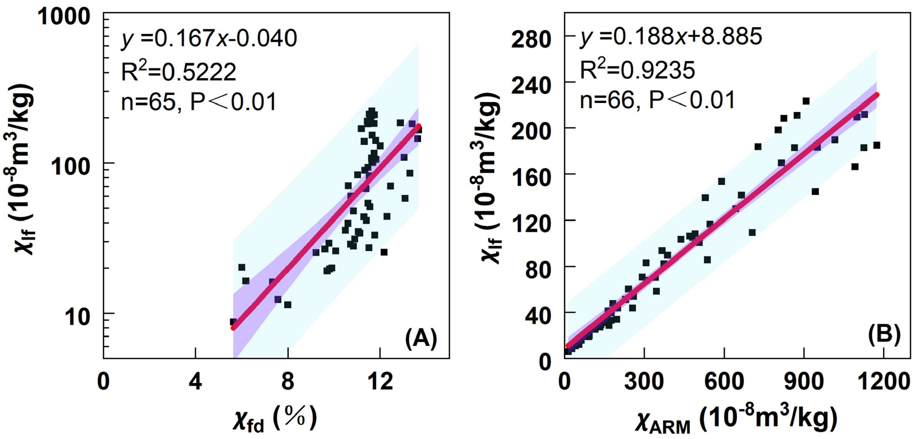

FIGURE 10
Relationships between χ_{lf} and **(A)** χ_{fd}%, **(B)** χ_{ARM}.

increase surface soil χ_{lf} by promoting the formation of Fe_o and hindering its aging.

5 Conclusion

The main characteristic of soil χ_{lf} profiles in the study area was a significantly higher χ_{lf} in the 0–80-cm soil layer relative to that in deep layers. χ_{lf} distribution was directly affected by Fe_o and indirectly affected by TN, SOC, pH, and EC. The main positive influence path was in the order of EC → SOC → TN → Fe_o → χ_{lf}, and the negative influence path followed pH → N → Feo → χ_{lf}. Denitrification and nitrification processes in the soil nitrogen cycle are usually coupled with iron redox reactions, with Fe_o forming under certain conditions. SOC and pH were the main factors promoting Fe_r weathering and Fe_c activation and its transformation into Fe_o. The ferrihydrite in Fe_o produced fine-grained magnetite and maghemite, the main ferrimagnetic minerals in soils in the study area, through dehydration, oxidation, and subsequent processes, leading to elevated χ_{lf} in the 0–80-cm soil layer. The results of this study serve as a reference for studying forest soils using χ_{lf}. Since χ_{lf} is strongly correlated with TN and SOC, its parameters hold promise for studying or predicting soil TN and SOC distribution.

Data availability statement

The datasets presented in this article are not readily available because the datasets used and/or analyzed during the current study available from the corresponding author on reasonable request. Requests to access the datasets should be directed to XZ, zhxl@kust.edu.cn.

Author contributions

XZ: Writing – original draft, Writing – review & editing. HW: Writing – original draft, Writing – review & editing. HoL: Investigation, Writing – review & editing. HaL: Writing – review & editing. YS: Software, Writing – original draft. GZ: Investigation, Writing – review & editing. FL: Investigation, Writing – review & editing. DL: Investigation, Writing – review & editing. XJ: Investigation, Writing – review & editing. ER: Investigation, Writing – review & editing. GL: Investigation, Writing – review & editing.

Funding

The author(s) declare that financial support was received for the research and/or publication of this article. This research was funded by the Yunnan Fundamental Research Projects (grant no. 202501AS070153).

Acknowledgments

We gratefully acknowledge Textcheck (a scientific and technical editing service) for revising the English language of the manuscript.

Conflict of interest

HoL was employed by the Yunnan Geology and Mining Engineering Survey Group Co., Ltd.

The remaining authors declare that the research was conducted in the absence of any commercial or financial relationships that could be construed as a potential conflict of interest.

Generative AI statement

The authors declare that no Gen AI was used in the creation of this manuscript.

Publisher's note

All claims expressed in this article are solely those of the authors and do not necessarily represent those of their affiliated organizations, or those of the publisher, the editors and the reviewers. Any product that may be evaluated in this article, or claim that may be made by its manufacturer, is not guaranteed or endorsed by the publisher.

References

Ajmal, Z., Muhmood, A., Usman, M., Kizito, S., Lu, J., Dong, R., et al. (2018). Phosphate removal from aqueous solutions using iron oxides: adsorption, desorption and regeneration characteristics. *J. Colloid Interface Sci.* 528, 145–155. doi: 10.1016/j.jcis.2018.05.084

Asgari, N., Ayoubi, S., and Demattê, J. A. M. (2018). Soil drainage assessment by magnetic susceptibility measures in western Iran. *Geoderma Reg.* 13, 35–42. doi: 10.1016/j.geodrs.2018.03.003

Ayoubi, S., Amiri, S., and Tajik, S. (2014). Lithogenic and anthropogenic impacts on soil surface magnetic susceptibility in an arid region of Central Iran. *Arch. Agron. Soil Sci.* 60, 1467–1483. doi: 10.1080/03650340.2014.893574

Ayoubi, S., and Mirsaidi, A. (2019). Magnetic susceptibility of entisol and aridisol great groups in southeastern Iran. *Geoderma Reg.* 16:e00202. doi: 10.1016/j.geodrs.2018.e00202

Ayoubi, Y., Wang, G., Liu, T., Shrestha, S., Xue, B., and Tan, Z. (2019). Vertical variations of soil water and its controlling factors based on the structural equation model in a semi-arid grassland. *Sci. Total Environ.* 691, 1016–1026. doi: 10.1016/j.scitotenv.2019.07.181

Banerjee, S. K., King, J., and Marvin, J. (1981). A rapid method for magnetic granulometry with applications to environmental studies. *Geophys. Res. Lett.* 8, 333–336. doi: 10.1029/GL008i004p00333

Bhattacharyya, A., Schmidt, M. P., Stavitski, E., and Martínez, C. E. (2018). Iron speciation in peats: chemical and spectroscopic evidence for the co-occurrence of ferric and ferrous iron in organic complexes and mineral precipitates. *Org. Geochem.* 115, 124–137. doi: 10.1016/j.orggeochem.2017.10.012

Bloemendal, J., Barton, C. E., and Radhakrishnamurthy, C. (1985). Correlation between Rayleigh loops and frequency-dependent and quadrature susceptibility: application to the magnetic granulometry of rocks. *J. Geophys. Res. Solid Earth* 90, 8789–8792. doi: 10.1029/jb090ib10p08789

Blume, H. P., and Schwertmann, U. (1969). Genetic evaluation of profile distribution of aluminum, iron, and manganese oxides. *Soil Sci. Soc. Am. J.* 33, 438–444. doi: 10.2136/sssaj1969.03615995003300030030x

Blundell, A., Dearing, J. A., Boyle, J. F., and Hannam, J. A. (2009). Controlling factors for the spatial variability of soil magnetic susceptibility across England and Wales. *Earth Sci. Rev.* 95, 158–188. doi: 10.1016/j.earscirev.2009.05.001

Borggaard, O. K. (1985). Organic matter and silicon in relation to the crystallinity of soil iron oxides. *Acta Agric. Scand.* 35, 398–406. doi: 10.1080/00015128509442051

Bremner, J. M., and Mulvaney, C. S. (1982). "Nitrogen-total" in Methods of soil analysis. Part 2. Chemical and microbiological properties. ed. A. L. Page (Madison: American Society of Agronomy, Soil Science Society of America), 595–624.

Calabrese, S., and Porporato, A. (2019). Impact of ecohydrological fluctuations on iron redox cycling. *Soil Biol. Biochem.* 133, 188–195. doi: 10.1016/j.soilbio.2019.03.013

Camargo, L. A., Marques, J., Pereira, G. T., Alleoni, L. R. F., Bahia, A. S. R. D., and Teixeira, D. D. (2016). Pedotransfer functions to assess adsorbed phosphate using iron oxide content and magnetic susceptibility in an Oxisol. *Soil Use and Management.* 32, 172–182. doi: 10.1111/sum.12255

César de Mello, D. C., Demattê, J. A. M., Silvero, N. E. Q., Di Raimo, L. A. D. L., Poppiel, R. R., Mello, F. A. O., et al. (2020). Soil magnetic susceptibility and its relationship with naturally occurring processes and soil attributes in pedosphere, in a tropical environments. *Geoderma* 372:114364. doi: 10.1016/j.geoderma.2020.114364

Chen, L. J., Li, C. S., Feng, Q., Wei, Y. P., Zhao, Y., Zhu, M., et al. (2019). Direct and indirect impacts of ionic components of saline water on irrigated soil chemical and microbial processes. *Catena* 172, 581–589. doi: 10.1016/j.catena.2018.09.030

Colombo, C., Palumbo, G., He, J. Z., Pinton, R., and Cesco, S. (2014). Review on iron availability in soil: interaction of Fe minerals, plants, and microbes. *J. Soils Sediments* 14, 538–548. doi: 10.1007/s11368-013-0814-z

Dearing, J. A., Hay, K. L., Baban, S. M. J., Huddleston, A. S., Wellington, E. M. H., and Loveland, P. J. (1996). Magnetic susceptibility of soil: an evaluation of conflicting theories using a national data set. *Geophys. J. Int.* 127, 728–734. doi: 10.1111/j.1365-246X.1996.tb04051.x

Delbecque, N., Van Ranst, E., Dondeyne, S., Mouazen, A. M., Vermeir, P., and Verdoodt, A. (2022). Geochemical fingerprinting and magnetic susceptibility to unravel the heterogeneous composition of urban soils. *Sci. Total Environ.* 847:157502. doi: 10.1016/j.scitotenv.2022.157502

Faměra, M., Kotková, K., Tůmová, Š., Elznicová, J., and Matys Grygar, T. (2018). Pollution distribution in floodplain structure visualized by electrical resistivity imaging in the Litavka River floodplain, the Czech Republic. *Catena* 165, 157–172. doi: 10.1016/j.catena.2018.01.023

Fine, P., Singer, M. J., Verosub, K. L., and TenPas, J. (1993). New evidence for the origin of ferrimagnetic minerals in loess from China. *Soil Sci. Soc. Am. J.* 57, 1537–1542. doi: 10.2136/sssaj1993.03615995005700060024x

Gasparatos, D., Massas, I., and Godelitsas, A. (2019). Fe-Mn concretions and nodules formation in redoximorphic soils and their role on soil phosphorus dynamics: Current knowledge and gaps. *Catena* 182:104106. doi: 10.1016/j.catena.2019.104106

Grison, H., Petrovsky, E., Kapicka, A., and Stejskalova, S. (2016). Magnetic and chemical parameters of andic soils and their relation to selected pedogenesis factors. *Catena* 139, 179–190. doi: 10.1016/j.catena.2015.12.005

Górka-Kostrubiec, B., Teisseyre-Jeleńska, M., and DytłOw, S. K. (2016). Magnetic properties as indicators of chernozem soil development. *Catena* 138, 91–102. doi: 10.1016/j.catena.2015.11.014

Grace, J. B., Michael Anderson, T. M., Smith, M. D., Seabloom, E., Andelman, S. J., Meche, G., et al. (2007). Does species diversity limit productivity in natural grassland communities? *Ecol. Lett.* 10, 680–689. doi: 10.1111/j.1461-0248.2007.01058.x

Hrouda, F. (2011). Models of frequency-dependent susceptibility of rocks and soils revisited and broadened. *Geophys. J. Int.* 187, 1259–1269. doi: 10.1111/j.1365-246X.2011.05227.x

Hu, X. F., Xu, L. F., Pan, Y., and Shen, M. N. (2009). Influence of the aging of Fe oxides on the decline of magnetic susceptibility of the tertiary red clay in the Chinese loess plateau. *Quat. Int.* 209, 22–30. doi: 10.1016/j.quaint.2009.02.019

Huang, R., Long, X. Y., Zhang, Y., Xing, D. C., Liu, C., Jiang, Y. J., et al. (2024). A dual mechanism drives the enrichment of pedogenic magnetic particles derived from red beds. *Catena* 246:108421. doi: 10.1016/j.catena.2024.108421

Ji, Y. P., Luo, W. Q., Lu, G. N., Fan, C., Tao, X. Q., Ye, H., et al. (2019). Effect of phosphate on amorphous iron mineral generation and arsenic behavior in paddy soils. *Sci. Total Environ.* 657, 644–656. doi: 10.1016/j.scitotenv.2018.12.063

Jiang, Z. X., Liu, Q. S., Roberts, A. P., Barrón, V., Torrent, J., and Zhang, Q. (2018). A new model for transformation of ferrihydrite to hematite in soils and sediments. *Geology* 46, 987–990. doi: 10.1130/G45386.1

Johnston, S. G., Morgan, B., and Burton, E. D. (2016). Legacy impacts of acid sulfate soil runoff on mangrove sediments: reactive iron accumulation, altered sulfur cycling and trace metal enrichment. *Chem. Geol.* 427, 43–53. doi: 10.1016/j.chemgeo.2016.02.013

Jordanova, N., Jordanova, D., and Petrov, P. (2016). Soil magnetic properties in Bulgaria at a national scale—challenges and benefits. *Glob. Planet. Change* 137, 107–122. doi: 10.1016/j.gloplacha.2015.12.015

Jörn, P., Lena, N., Novothny, Á., Gabriella, B., Christian, R., Manfred, F., et al, (2018). Paleoenvironmental conditions and sedimentation dynamics in central europe inferred from geochemical data of the loess-paleosol sequence at Süttő (hungary).*Quat. Sci. Rev.* 196, 21–37.

Kanu, M. O., Meludu, O. C., Basavaiah, N., and Joseph, G. (2023). The use of environmental magnetic properties, elemental analysis, and geostatistical tools for soil pollution assessment, a lesson from Takum, Nigeria. *Phys. Chem. Earth Pt. A B C.* 130:103377. doi: 10.1016/j.pce.2023.

Karimi, A., Haghnia, G. H., Ayoubi, S., and Safari, T. (2017). Impacts of geology and land use on magnetic susceptibility and selected heavy metals in surface soils of Mashhad plain, northeastern Iran. *J. Appl. Geophys.* 138, 127–134. doi: 10.1016/j.jappgeo.2017.01.022

Kirana, K. H., Hutabalian, M. A., Fitriani, D., Agustine, E., Hamdan, A. M., and Rosandi, Y. (2024a). Magnetic characterization of soils in the landslide area (case study: Cihanjuang village, Sumedang, West Java). *IOP Conf. Ser. Earth Environ. Sci.* 1432:012001. doi: 10.1088/1755-1315/1432/1/012001

Kirana, K. H., Shalsabila, M. T., Putri, S. U., Fitriani, D., Agustine, E., Hamdan, A. M., et al. (2024b). Topsoil's magnetic and electrical properties in a volcanic and tropical region. *Environ. Monit. Assess.* 196:160. doi: 10.1007/s10661-024-12332-8

Li, Y. C., Li, Y. T., Li, L. F., Tang, M. D., Wang, Y. H., and Ai, S. Y. (2018a). Mechanisms of the iron-nitrogen coupled cycles controlling variations of cadmium activity in paddy soil. *Acta Sci. Circum.* 38, 328–335. doi: 10.13671/j.hjkxxb.2017.0272

Li, Z. H., Wei, B. M., Wang, X. D., Zhang, Y. L., and Zhang, A. F. (2018b). Responses of soil organic carbon fractions and CO_2 emissions to exogenous composted manure and calcium carbonate. *J. Soils Sediments* 18, 1832–1843. doi: 10.1007/s11368-018-1946-y

Li, Y., Yu, S., Strong, J., and Wang, H. (2012). Are the biogeochemical cycles of carbon, nitrogen, sulfur, and phosphorus driven by the FeIII–-FeII redox wheel in dynamic redox environments? *J. Soils Sediments* 12, 683–693. doi: 10.1007/s11368-012-0507-z

Li, R. F., Zhang, X. H., Ji, W. J., He, X. L., and Li, Z. (2024). Multivariate and scale-dependent controls of deep soil carbon after afforestation in a typical loess-covered region. *J. Environ. Manag.* 359:120998. doi: 10.1016/j.jenvman.2024.120998

Li, Y., Zhang, H., Tu, C., and Luo, Y. (2017). Magnetic characterization of distinct soil layers and their implications for environmental changes in coastal soils of the Yellow River Delta. *Catena* 162, 245–254. doi: 10.1016/j.catena.2017.11.006

Lindsay, W. L. (1991). Iron oxide solubilization by organic matter and its effect on iron availability. *Plant Soil* 130, 27–34. doi: 10.1007/BF00011852

Liu, C., Deng, C., and Liu, Q. (2012). Mineral magnetic studies of the vermiculated red soils in Southeast China and their paleoclimatic significance. *Palaeogeogr. Palaeoclimatol. Palaeoecol.* 330, 173–183. doi: 10.1016/j.palaeo.2012.02.035

Liu, X., Qin, J. F., Yang, J. S., Zhang, J. P., Yang, Y. F., Sun, D. D., et al. (2023). Response of soil iron oxides in freshwater marshes to different tidal hydrologies in the Yellow River estuary wetland, China. *Ecol. Eng.* 190:106942. doi: 10.1016/j.ecoleng

Liu, Q. S., Roberts, A. P., Larrasoaña, J. C., Banerjee, S. K., Guyodo, Y., Tauxe, L., et al. (2012). Environmental magnetism: principles and applications. *Rev. Geophys.* 50:393. doi: 10.1029/2012RG000393

Liu, L., Zhang, Z., Zhang, K., Liu, H., and Fu, S. (2018). Magnetic susceptibility characteristics of surface soils in the Xilingele grassland and their implication for soil redistribution in wind-dominated landscapes: a preliminary study. *Catena* 163, 33–41. doi: 10.1016/j.catena.2017.12.009

Lizaga, I., Quijano, L., Gaspar, L., and Navas, A. (2019). Linking land use changes to variations in soil properties in a Mediterranean mountain agroecosystem. *Catena* 172, 516–527. doi: 10.1016/j.catena.2018.09.019

Lu, S. G. (2000). Lithological factors affecting magnetic susceptibility of subtropical soils, Zhejiang Province, China. *Catena* 40, 359–373. doi: 10.1016/S0341-8162(00)00092-8

Magiera, T., Łukasik, A., Zawadzki, J., and Rösler, W. (2019). Magnetic susceptibility as indicator of anthropogenic disturbances in forest topsoil: a review of magnetic studies carried out in central European forests. *Ecol. Indic.* 106:105518. doi: 10.1016/j.ecolind.2019.105518

Maher, B. A. (1998). Magnetic properties of modern soils and quaternary loessic paleosols: Paleoclimatic implications. *Palaeogeogr. Palaeoclimatol. Palaeoecol.* 137, 25–54. doi: 10.1016/S0031-0182(97)00103-X

Maher, B. A., Alekseev, V., and Alekseev, T. (2003). Magnetic mineralogy of soils across the Russian steppe: climatic dependence of pedogenic magnetite formation. *Palaeogeogr. Palaeoclimatol. Palaeoecol.* 210, 321–341. doi: 10.1016/S0031-0182(03)00618-7

Maher, B. A., and Taylor, R. M. (1988). Formation of ultrafine-grained magnetite in soils. *Nature* 336, 368–370. doi: 10.1038/336368a0

Manna, L. L., Gaspar, L., Rostagno, C. M., Quijano, L., and Navas, A. (2018). Soil changes associated with land use in Patagonic volcanic soils have developed in dynamic landscapes. *Catena* 166, 229–239. doi: 10.1016/j.catena.2018.03.025

Marques, J., Siqueira, D. S., Camargo, L. A., Teixeira, D. D. B., Barrón, V., and Torrent, J. (2014). Magnetic susceptibility and diffuse reflectance spectroscopy to characterize the spatial variability of soil properties in a Brazilian haplustalf. *Geoderma* 219, 63–71. doi: 10.1016/j.geoderma.2013.12.007

McKeague, J. A., Brydon, J. E., and Miles, N. M. (1971). Differentiation of forms of extractable iron and aluminum in soil. *Soil Sci. Soc. Am. J.* 35, 33–38. doi: 10.2136/sssaj1971.03615995003500010016x

McKeague, J. A., and Day, J. H. (1966). Dithionite- and oxalate-extractable Fe as aids in differentiating various classes of soils. *Can. J. Soil Sci.* 46, 13–22. doi: 10.4141/cjss66-003

Mehra, O. P., and Jackson, M. L. (1958). Iron oxide removal from soils and clays by a dithionite-citrate system buffered with sodium bicarbonate. *Clay Clay Miner.* 7, 317–327. doi: 10.1346/CCMN.1958.0070122

Melton, E. D., Swanner, E. D., Behrens, S., Schmidt, C., and Kappler, A. (2014). The interplay of microbially mediated and abiotic reactions in the biogeochemical Fe cycle. *Nat. Rev. Microbiol.* 12, 797–808. doi: 10.1038/nrmicro3347

Mullins, C. E. (1977). Magnetic susceptibility of soil and its significance in soil science: a review. *Eur. J. Soil Sci.* 28, 223–246. doi: 10.1111/j.1365-2389.1977.tb02232.x

Oldfield, F. (1991). Environmental magnetism–a personal perspective. *Quat. Sci. Rev.* 10, 73–85. doi: 10.1016/0277-3791(91)90031-O

Owliaie, H. R., and Ghiri, M. N. (2018). The magnetic susceptibility and iron oxides of aquic soils in southern Iran. *Eurasian Soil Sci.* 51, 1252–1265. doi: 10.1134/S1064229318100095

Pallud, C., Kausch, M., Fendorf, S., and Meile, C. (2010). Spatial patterns and modeling of reductive ferrihydrite transformation observed in artificial soil aggregates. *Environ. Sci. Technol.* 44, 74–79. doi: 10.1021/es901736t

Pérez, I., Romero, F. M., Zamora, O., and Gutiérrez-Ruiz, M. E. (2014). Magnetic susceptibility and electrical conductivity as a proxy for evaluating soil contaminated with arsenic, cadmium and lead in a metallurgical area in the San Luis Potosi state, Mexico. *Environ. Earth Sci.* 72, 1521–1531. doi: 10.1007/s12665-014-3057-4

Pizarro, C., Escudey, M., and Fabris, J. D. (2003). Influence of organic matter on the iron oxide mineralogy of volcanic soils. *Hyperfine Interact.* 148–149, 53–59. doi: 10.1023/B:HYPE.0000003764.17385.a9

Poggere, G. C., Inda, A. V., Barrón, V., KäMpf, N., de Brito, A. D. B., Barbosa, J. Z., et al. (2018). Maghemite quantification and magnetic signature of Brazilian soils with contrasting parent materials. *Appl. Clay Sci.* 161, 385–394. doi: 10.1016/j.clay.2018.05.014

Preetz, H., Igel, J., Hannam, J. A., and Stadler, S. (2017). Relationship between magnetic properties and reddening of tropical soils as indicators of weathering. *Geoderma* 303, 143–149. doi: 10.1016/j.geoderma.2017.05.007

Profe, J., Neumann, L., Novothny, Á., Barta, G., Rolf, C., Frechen, M., et al. (2018). Paleoenvironmental conditions and sedimentation dynamics in Central Europe inferred from geochemical data of the loess-paleosol sequence at Süttő (Hungary). *Quat. Sci. Rev.* 196, 21–37. doi: 10.1016/j.quascirev.2018.07.034

Putri, M. Y., Sudarningsih, S., Fahruddin, F., Ibrahim, I., Rifai, H., and Hamdan, M. A. (2024). Susceptibility and metallics elements in soil struck by lightning in west Kotawaringin regency, Central Kalimantan. *Phys. Conf. Ser.* 2866:012068. doi: 10.1088/1742-6596/2866/1/012068

Quijano, L., Chaparro, M. A. E., Marie, D. C., Gaspar, L., and Navas, A. (2014). Relevant magnetic and soil parameters as potential indicators of soil conservation status of Mediterranean agroecosystems. *Geophys. J. Int.* 198, 1805–1817. doi: 10.1093/gji/ggu239

Rahimi, M. R., Ayoubi, S., and Abdi, M. R. (2013). Magnetic susceptibility and cs-137 inventory variability as influenced by land use change and slope positions in a hilly, semiarid region of west-Central Iran. *J. Appl. Geophys.* 89, 68–75. doi: 10.1016/j.jappgeo.2012.11.009

Ramdhani, R., Fitriani, D., Kirana, K. H., Wijatmoko, B., and Sutanto, O. (2016). Magnetic properties of soils from landslide potential areas (case study: Pasir Ipis-Lembang, West Bandung). *J. Phys. Conf. Ser.* 739:012107. doi: 10.1088/1742-6596/739/1/012107

Rochette, P. (1987). Magnetic susceptibility of the rock matrix related to magnetic fabric studies. *J. Struct. Geol.* 9, 1015–1020. doi: 10.1016/0191-8141(87)90009-5

Sadiki, A., Faleh, A., Navas, A., and Bouhlassa, S. (2009). Using magnetic susceptibility to assess soil degradation in the eastern Rif, Morocco. *Earth Surf. Process. Landforms* 34, 2057–2069. doi: 10.1002/esp.1891

Sarmast, M., Farpoor, M. H., and Boroujeni, I. E. (2017). Magnetic susceptibility of soils along a lithotoposequence in southeastern Iran. *Catena* 156, 252–262. doi: 10.1016/j.catena.2017.04.019

Schwertmann, U. (1985). "Effect of pedogenic environments on iron oxide minerals" in Advances in soil science. ed. B. A. Stewart (New York, NY: Springer).

Schwertmann, U. (1988). "Occurrence and formation of iron oxides in various pedoenvironments" in Iron in soil and clay minerals. eds. J. W. Stucki, B. A. Goodman and U. Schwertmann (Dordrecht: D. Reidel), 267–308.

Shi, Y. J., Xu, L., Zhou, Y. F., Ji, B. Y., Zhou, G. M., Fang, H. Y., et al. (2018). Quantifying driving factors of vegetation carbon stocks of Moso bamboo forests using machine learning algorithm combined with structural equation model. *For. Ecol. Manag.* 429, 406–413. doi: 10.1016/j.foreco.2018.07.035

Su, N., Yang, S. Y., Wang, X. D., Bi, L., and Yang, C. F. (2015). Magnetic parameters indicate the intensity of chemical weathering developed on igneous rocks in China. *Catena* 133, 328–341. doi: 10.1016/j.catena.2015.06.003

Sudarningsih, S., Fahruddin, F., Astuti, P., Wahyono, S. C., Ibrahim, I., Siregar, S. S., et al. (2024). Integrated magnetic and geochemical assessment of the soil from the steam power plant area of South Kalimantan Province 13th international physics seminar. *J. Phys. Conf. Ser.* 2866:012065. doi: 10.1088/1742-6596/2866/1/012065

Sudarningsih, S., Pratama, A., Bijaksana, S., Fahruddin, F., Zanuddin, A., Salim, A., et al. (2023). Magnetic susceptibility and heavy metal content in sediments of Riam Kiwa, Riam Kanan and Martapura Rivers, Kalimantan Selatan Province, Indonesia. *Heliyon* 9:e16425. doi: 10.1016/j.heliyon.2023.e16425

Taylor, R. M., Maher, B. A., and Self, P. G. (1987). Magnetite in soils: I. The synthesis of single-domain and superparamagnetic magnetite. *Clay Miner.* 22, 411–422. doi: 10.1180/claymin.1987.022.4.05

Torrent, J., Barrón, V., and Liu, Q. (2006). Magnetic enhancement is linked to and precedes hematite formation in aerobic soil. *Geophys. Res. Lett.* 33:L02401. doi: 10.1029/2005GL024818

Torrent, J., Liu, Q. S., and Barrón, V. (2010). Magnetic susceptibility changes in relation to pedogenesis in a Xeralf chronosequence in northwestern Spain. *Eur. J. Soil Sci.* 61, 161–173. doi: 10.1111/j.1365-2389.2009.01216.x

Wang, J. S., Grimley, D. A., Xu, C., and Dawson, J. O. (2008). Soil magnetic susceptibility reflects soil moisture regimes and the adaptability of tree species to these regimes. *For. Ecol. Manag.* 255, 1664–1673. doi: 10.1016/j.foreco.2007.11.034

Wang, S., Lin, S., and Lu, S. (2013). Rock magnetism, iron oxide mineralogy, and geochemistry of the quaternary red earth in Central China and their paleopedogenic implications. *Palaeogeogr. Palaeoclimatol. Palaeoecol.* 379, 95–103. doi: 10.1016/j.palaeo.2013.04.010

Wang, B., Xia, D., Yu, Y., Chen, H., and Jia, J. (2018). Source apportionment of soil contamination in Baotou City (North China) based on a combined magnetic and geochemical approach. *Sci. Total Environ.* 642, 95–104. doi: 10.1016/j.scitotenv.2018.06.050

Winkler, P., Kaiser, K., Thompson, A., Kalbitz, K., Fiedler, S., and Jahn, R. (2018). Contrasting evolution of iron phase composition in soils exposed to redox fluctuations. *Geochim. Cosmochim. Acta* 235, 89–102. doi: 10.1016/j.gca.2018.05.019

Xiao, S. S., Ye, Y. Y., Xiao, D., Chen, W. R., Zhang, W., and Wang, K. L. (2019). Effects of tillage on soil N availability, aggregate size, and microbial biomass in a subtropical karst region. *Soil Till. Res.* 192, 187–195. doi: 10.1016/j.still.2019.05.006

Xu, M. M., Zhao, Z. J., Shi, M., Yao, L. W., Fan, T. F., and Wang, Z. M. (2019). Effect of humic acid on the stabilization of cadmium in soil by coprecipitating with ferrihydrite. *Environ. Sci. Pollut. Res. Int.* 26, 27330–27337. doi: 10.1007/s11356-019-05893-6

Zhang, M. J., Zhang, W., Zhang, K.l., Yu, Y., and Liu, L. (2023). Centennial scale temporal responses of soil magnetic susceptibility and spatial variation to human cultivation on hillslopes in Northeast China. *Soil Tillage Res.* 234:105865. doi: 10.1016/j.still.2023.105865

Zhang, J. B., Zhu, T. B., Cai, Z. C., and Müller, C. (2011). Nitrogen cycling in forest soils across climate gradients in eastern China. *Plant Soil* 342, 419–432. doi: 10.1007/s11104-010-0706-6